Supporting Information

Alcohol-Mediated Self-Assembly of Mesoporous Transition-Metal Pyrophosphates and Phosphates: Transformation to Metal Hydroxides and Alkaline OER Performance

Gözde Ceran[a], Irmak Karkaya Durukan,[a] and Ömer Dag[a,b]

[a]Department of Chemistry, Bilkent University, 06800, Ankara, Turkey

[b]UNAM — National Nanotechnology Research Center and Institute of Materials Science and Nanotechnology, Bilkent University, 06800, Ankara, Turkey.
Email: dag@fen.bilkent.edu.tr

Table S1. Amounts of ingredients used for the initial 30Co(II)-15PPA-P123, 30Ni(II)-15PPA-P123, 30Ni(II)-15PPA-P123 solutions (.

Solutions	**P123 (g)**	**Salts (g)**			**PPA (g)**	**Solvents (mL)**		
		Co(II)	**Ni(II)**	**Mn(II)**		**Metanol**	**Ethanol**	**Butanol**
30Co(II)-	1.000	1.518			0.465	10	-	-
15PPA-P123	1.000	1.518			0.465	-	10	-
	1.000	1.518			0.465	-	-	10
30Ni(II)-	1.000		1.490		0.460	10		
15PPA-P123	1.000		1.490		0/460		10	
	1.000		1.490		0.460			10
30Mn(II)-	1.000			1.295	0.457	10	-	-
15PPA-P123	1.000			1.295	0.457	-	10	-
	1.000			1.295	0.457	-	-	10

Table S2. BET Surface Area, BJH Pore Width, and Pore Volume Comparison of $Co_2P_2O_7$, $Ni_2P_2O_7$, and $Mn_2P_2O_7$.

Sample	BET surface Area/ m^2/g	Pore Width/nm	Pore Volume/cm^3/g	Reference
$Co_2P_2O_7$	16.1	10-70	-	1
$Co_2P_2O_7$	47	15	-	2
$Co_2P_2O_7$/MWCT	109.8	1-25	0.54	3
$Co_2P_2O_7$-NC-2	13.2	12.63	0.05	4
$Co_2P_2O_7$ Nanowires	234.5	3-30	-	5
$Co_2P_2O_7$-LLC	49	8.5		6
$Ni_2P_2O_7$	36	-	-	7
Na-doped $Ni_2P_2O_7$	190	2-4	-	8
$Ni_2P_2O_7$	30	-	-	9
$Ni_2P_2O_7$	6	11		10
$Ni_2P_2O_7$	45	-	0.13	11
$Ni_2P_2O_7$-LLC	60	10.8	-	12
$Ni_2P_2O_7$	95	2	–	13
$Ni_2P_2O_7$/RGO	176	8	-	13
$Mn_2P_2O_7$	54	30.3	-	14
$Mn_2P_2O_7$@PPy	93	20.2	-	14
$Mn_2P_2O_7$	15.6	-	-	15
$Mn_2P_2O_7$-LLC	39	10.5	-	6

Table S3. Overpotential and Tafel Slope comparison.

Electrode Material/Substrate	j (mA/cm^2)	KOH Conc. (M)	Overpotential (mV)	Tafel Slope (mV/dec)	Reference
G-Co_3O_4	10	1	313	56	16
Co_3O_4 NCs	10	1	415	53	17
$NiCo_{2.7}(OH)_x$	10	1	350	65	18
CoFe/C	10	1	300	61	17
NiCo-LDH	10	1	420	113	19
CoFe LDH HNC	10	1	238	48	20
$Ni(OH)_2$-MD/Carbon Paper	10	1	300	104	21
β-$Ni(OH)_2$/Carbon Paper	10	1	380	153	21
NiFe-SW/Glassy Carbon	12	1	250	38.9	22
NiFe Film/Nickel Foam	24	1	250	-	23
α-$Ni(OH)_2$/Glassy Carbon	10	0.1	331	-	24
Ni-Fe Oxide/Carbon Paper	10	1	303	58.5	25
$Ni_{1-x}Mn_xO$/Graphite	10	1	311	48	26
$Ni(OH)_2$-NiPP/Graphite	100	1	381	45	27
α-MnO_2	10	1	490	87.7	28
β-MnO_2	10	1	550	90	29
MnOOH@$CD_{0.2}$	10	1	232	51.3	30
α-Mn_2O_3/FTO	10	1	340	-	31
β-MnOOH/NF	10	1	395	66	32
Defective δ-MnO_2 nanosheets	10	1	320	40	33
$CoMn_2O_4$-120	10	1	292	47	34
$Ni_{0.2}$-Co_3O_4-V_O NRs	10	1	291	92.7	35
δ-NiOOH	100	1	201	46.3	36
S-$NiCoFe(OH)_x$/NF	100	1	283	36.2	37
NiO/CNT, RuO_2/NiO/CNT	10	1	320/208	159/115	38

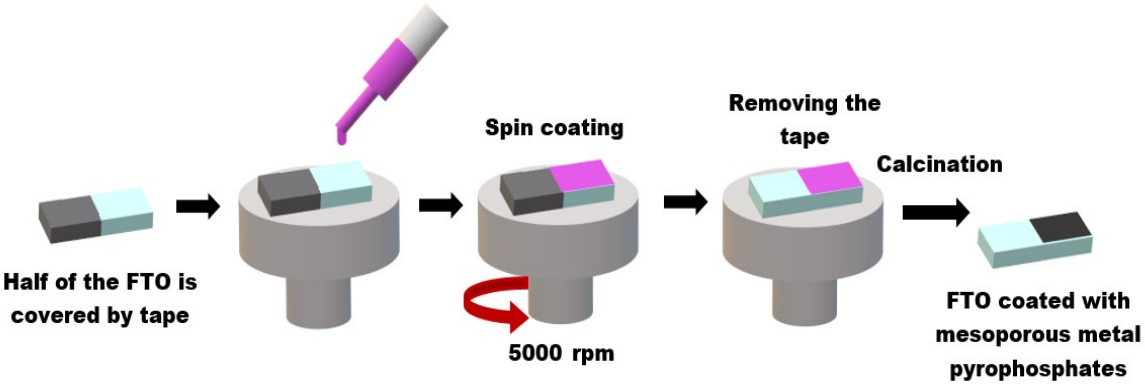

Scheme S1. Schematic representation of the spin-coating process of the solutions and supernatants and preparation of FTO coated electrodes.

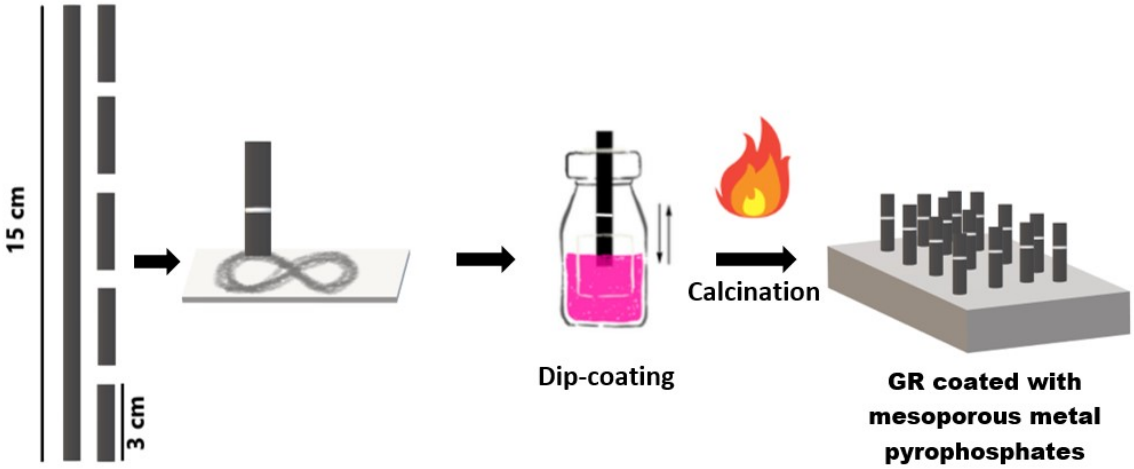

Scheme S2. Schematic representation of the dip-coating process of the solutions and supernatants and preparation of graphite coated electrodes.

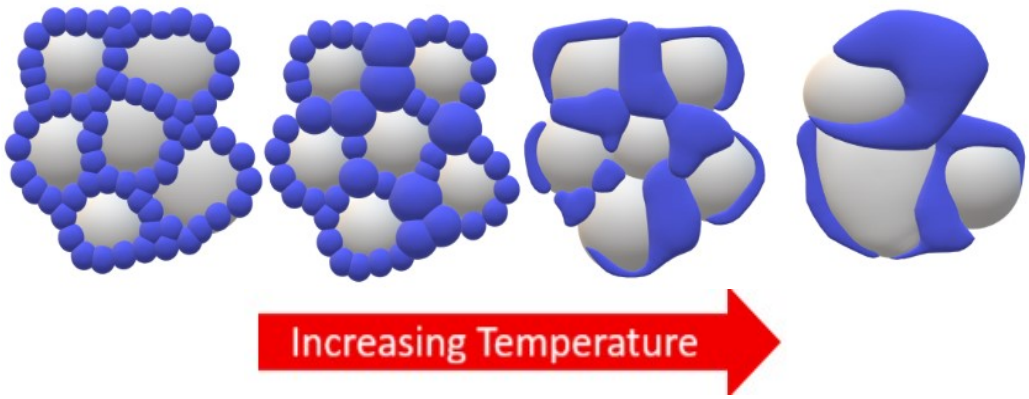

Scheme S3. A schematic representation of the change in the porosity upon increasing annealing temperature of the $M_2P_2O_7$ samples (blue spheres represent $M_2P_2O_7$ particles/pore-wall and light gray spheres are the pores).

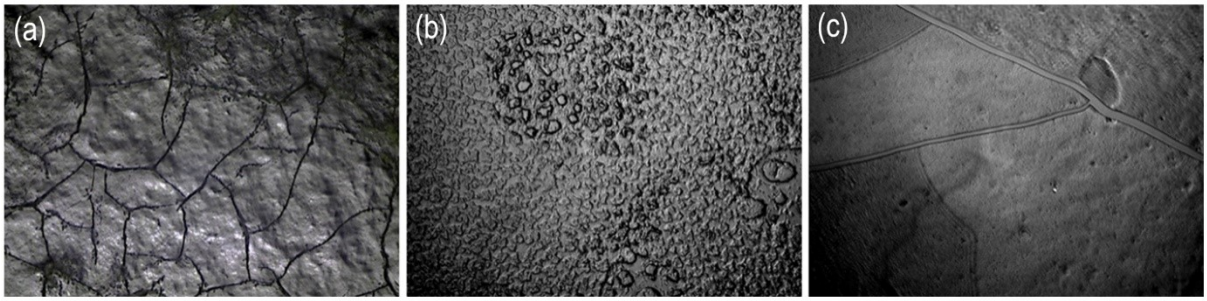

Figure S1. POM images of the nickel samples, coated over glass slides and aged at room temperature: (a) ethanol solution, (b) supernatant, and (c) precipitate fractions.

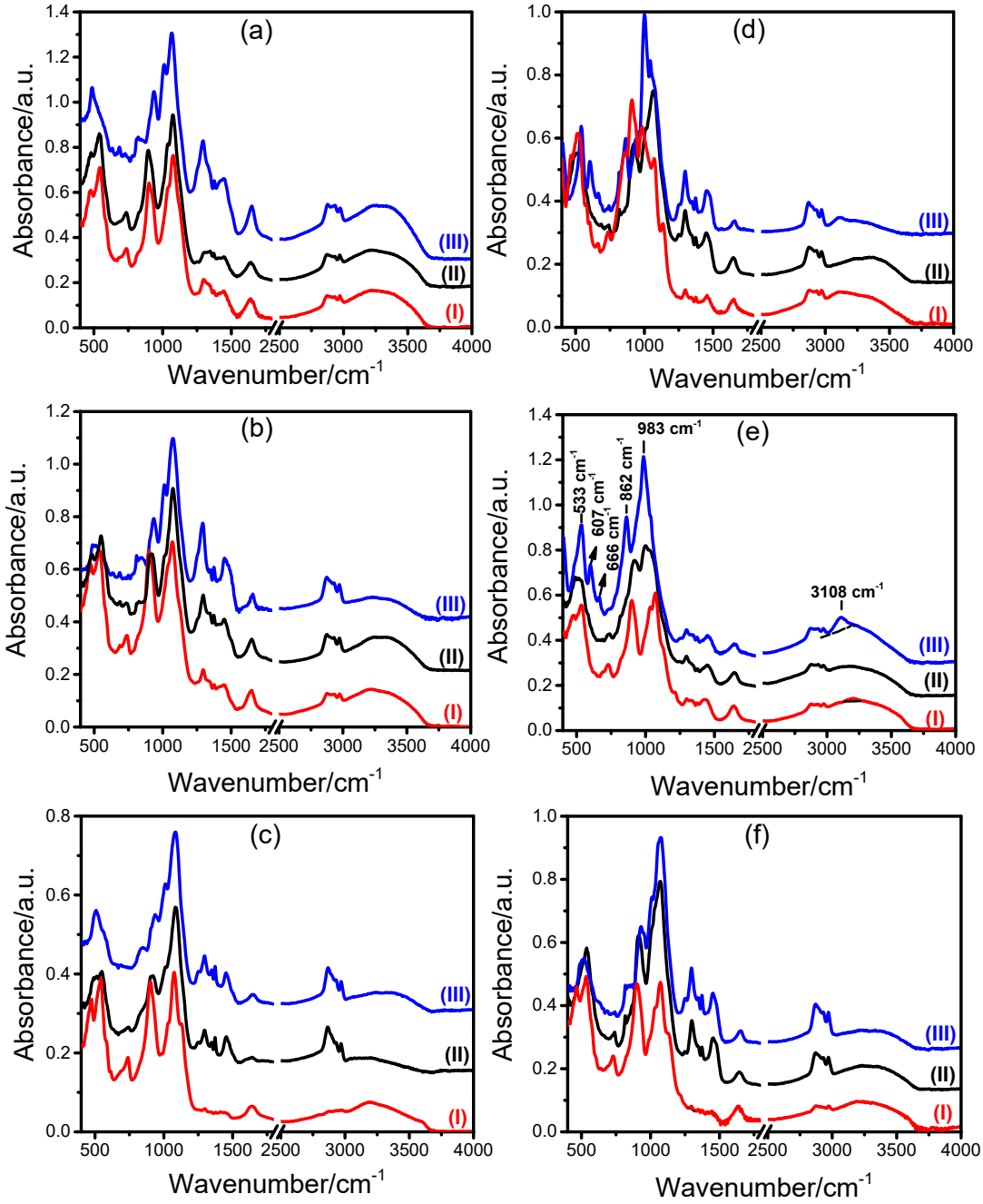

Figure S2. ATR-FTIR spectra of 24 h-aged (a, b, and c) Co(II)-PPA-P123 and (d, e, and f) Mn(II)-PPA-P123 samples: from (a and d) butanol, (b and e) ethanol, and (c and f) methanol of the precipitate (I), supernatant (II), and solution (III) portions.

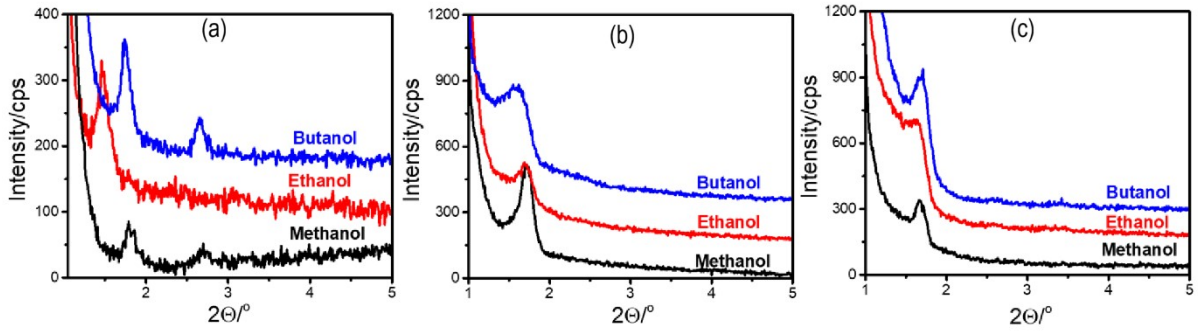

Figure S3. Small angle XRD patterns: (a) Co(II), (b) Mn(II), and (c) Ni(II), after 5 hrs aging of butanol, ethanol and methanol supernatants.

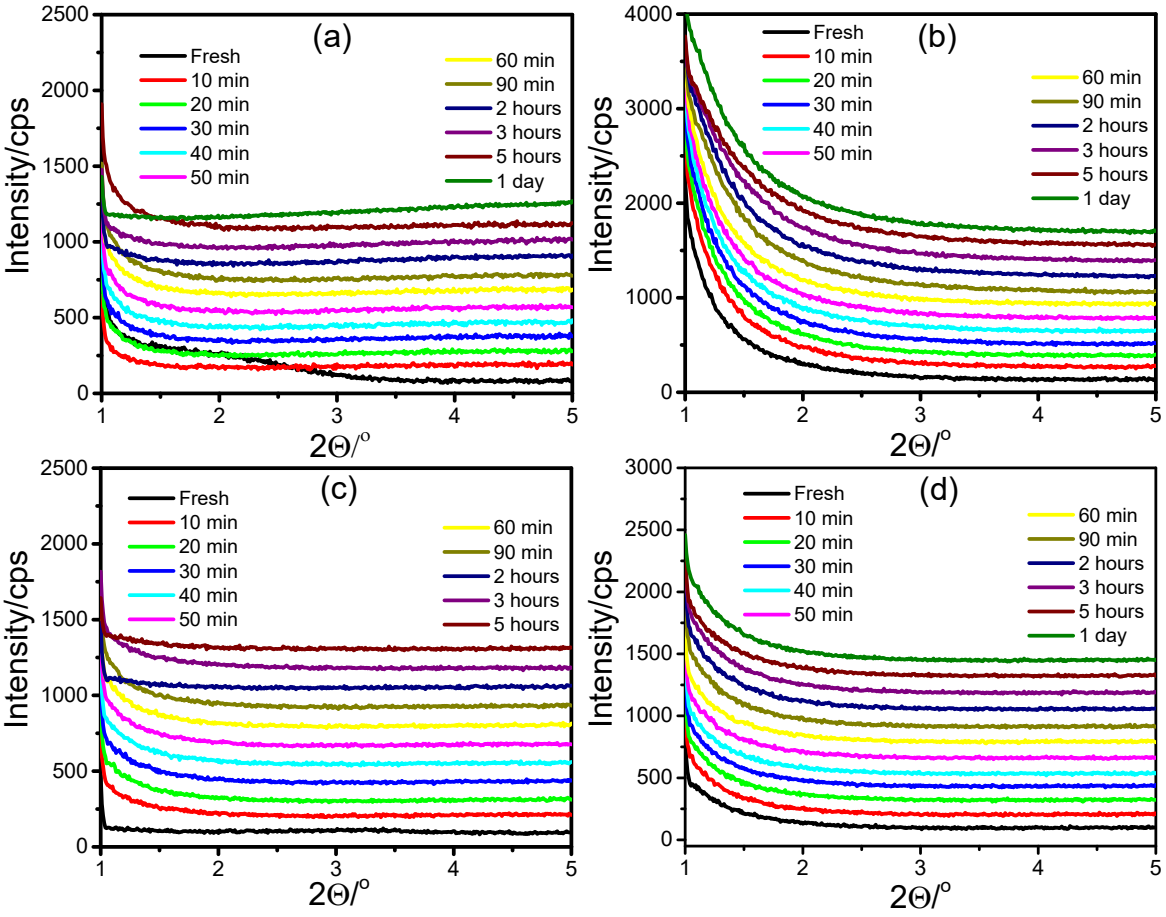

Figure S4. Small-angle XRD patterns of (a, b) Ni(II)-PPA-P123 and (c, d) Mn(II)-PPA-P123 ethanol samples during aging of the solution (a, c) and precipitate (b,d) fractions.

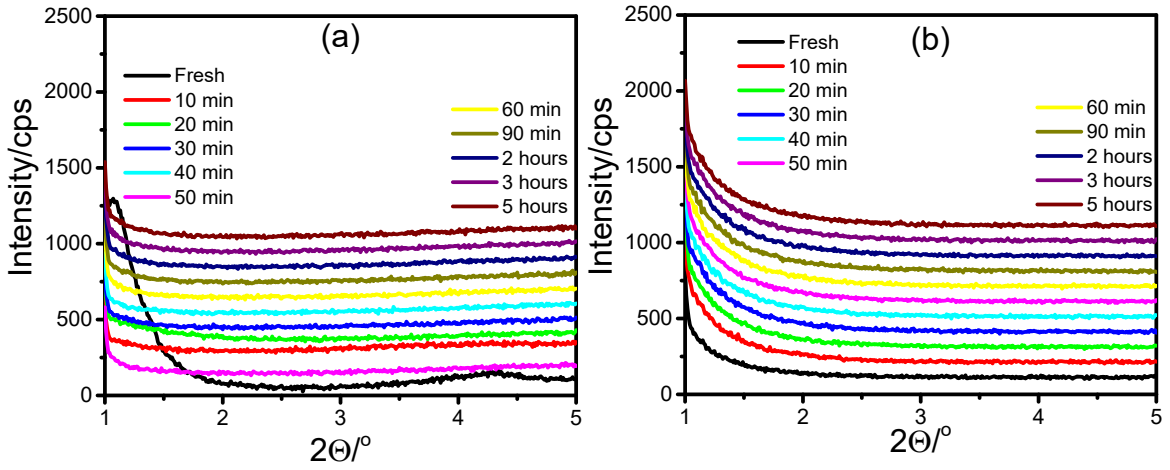

Figure S5. Small-angle XRD patterns of (a) solution and (b) precipitate fractions from Co(II)-PPA-P123-Butanol during aging.

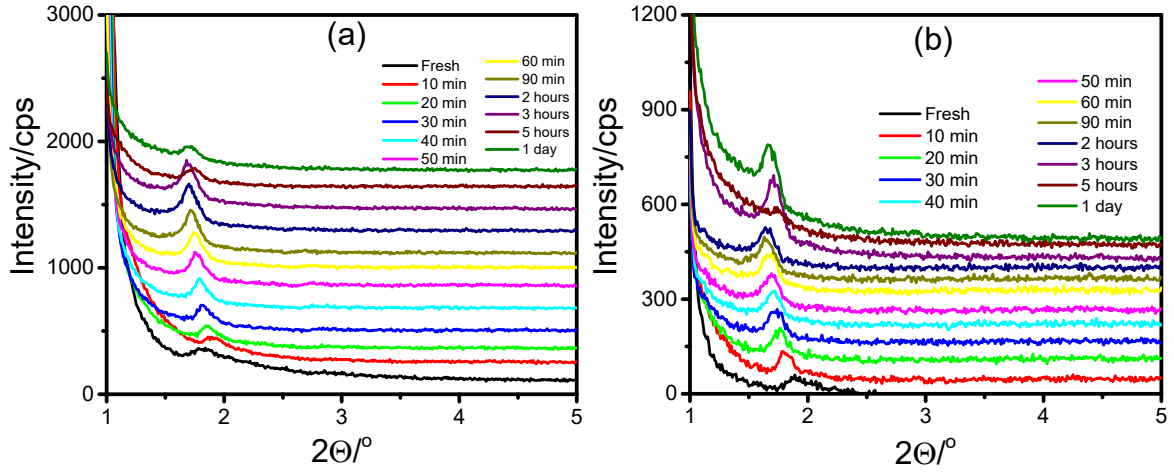

Figure S6. Small angle XRD patterns: (a) Ni(II):PPA:P123-Methanol solution and (b) Ni(II):PPA:P123-Methanol supernatant during aging.

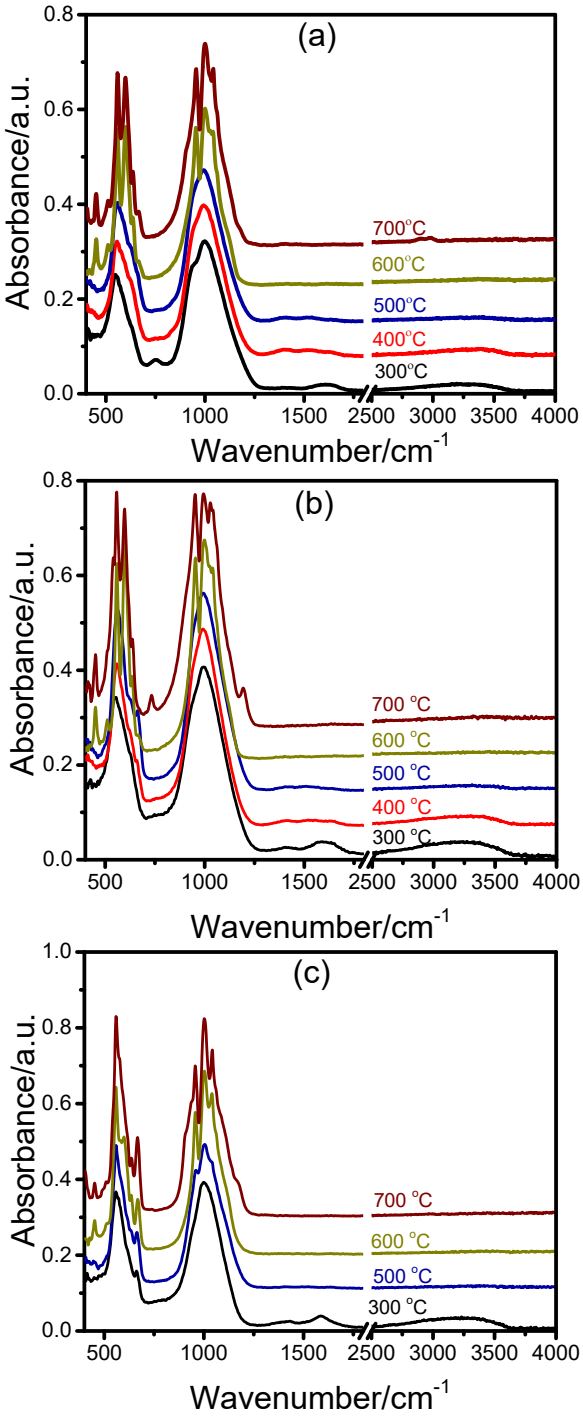

Figure S7. ATR-FTIR spectral changes with increasing annealing temperature of $Co_3(PO_4)_2$, obtained from (a) methanol, (b) ethanol, and (c) butanol supernatants. (d) XRD pattern of $Co_3(PO_4)_2$, annealed at 700 °C and reference pattern (ICDD 00-013-0503).

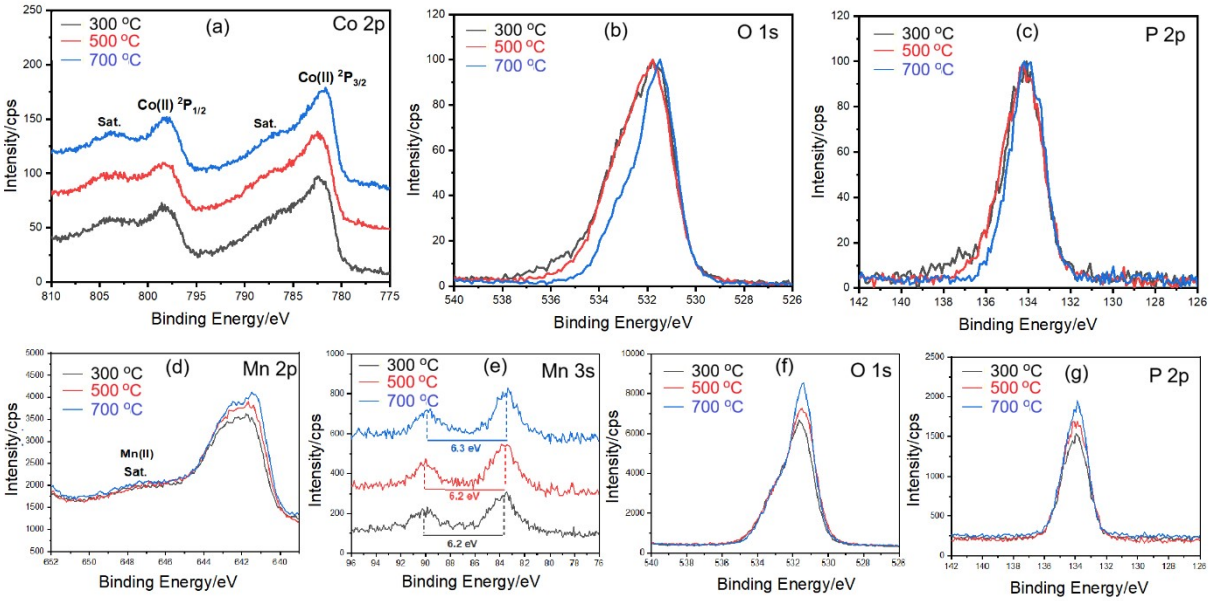

Figure S8. XPS spectra: (a) Co 2p, (b) O 1s, and (c) P 2p, regions of $Co_2P_2O_7$, (d) Mn 2p, (e) Mn 3s, (f) O1s, and (g) P 2p regions of $Mn_2P_2O_7$, calcined at 300, 500, and 700 °C.

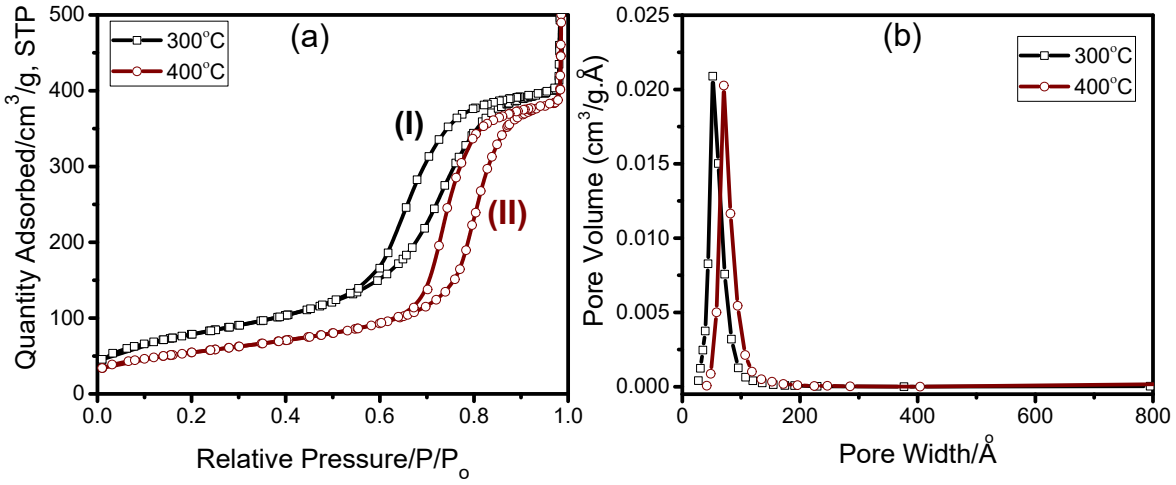

Figure S9. (a) 77(K) N_2 adsorption-desorption isotherms and (b) BJH pore size distribution plots of $Ni_3(PO_4)_2$ from butanol supernatant fraction calcined at (I) 300 and (II) 400 °C.

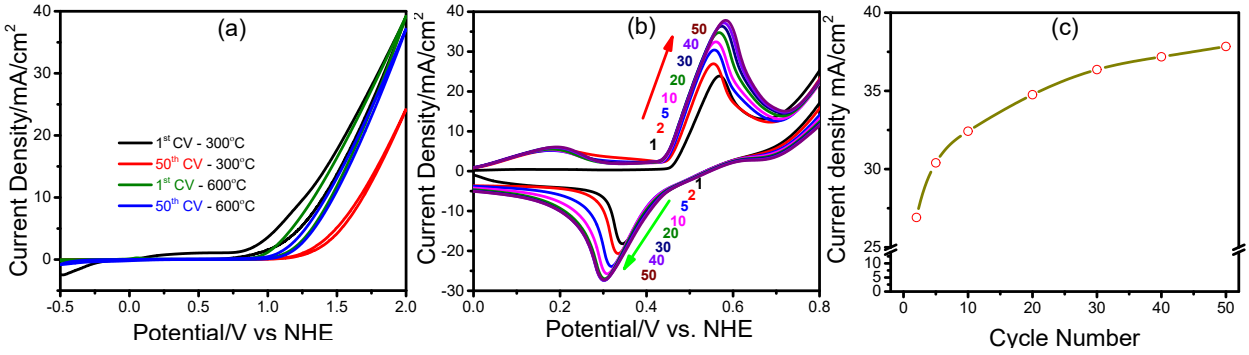

Figure S10. (a) 1st and 50th CVs of the $Co_2P_2O_7$ coated GR electrode, calcined at 300 and 600 ºC, (b) the selected group of CVs from the 50 CV cycles (numbers are cycle numbers) of the $Ni_2P_2O_7$ coated GR electrode in the 0.0 and 0.8 V potential window, and (c) The change in the current density at the oxidation peak as a function of cycle number of the same electrode in pannel (b).

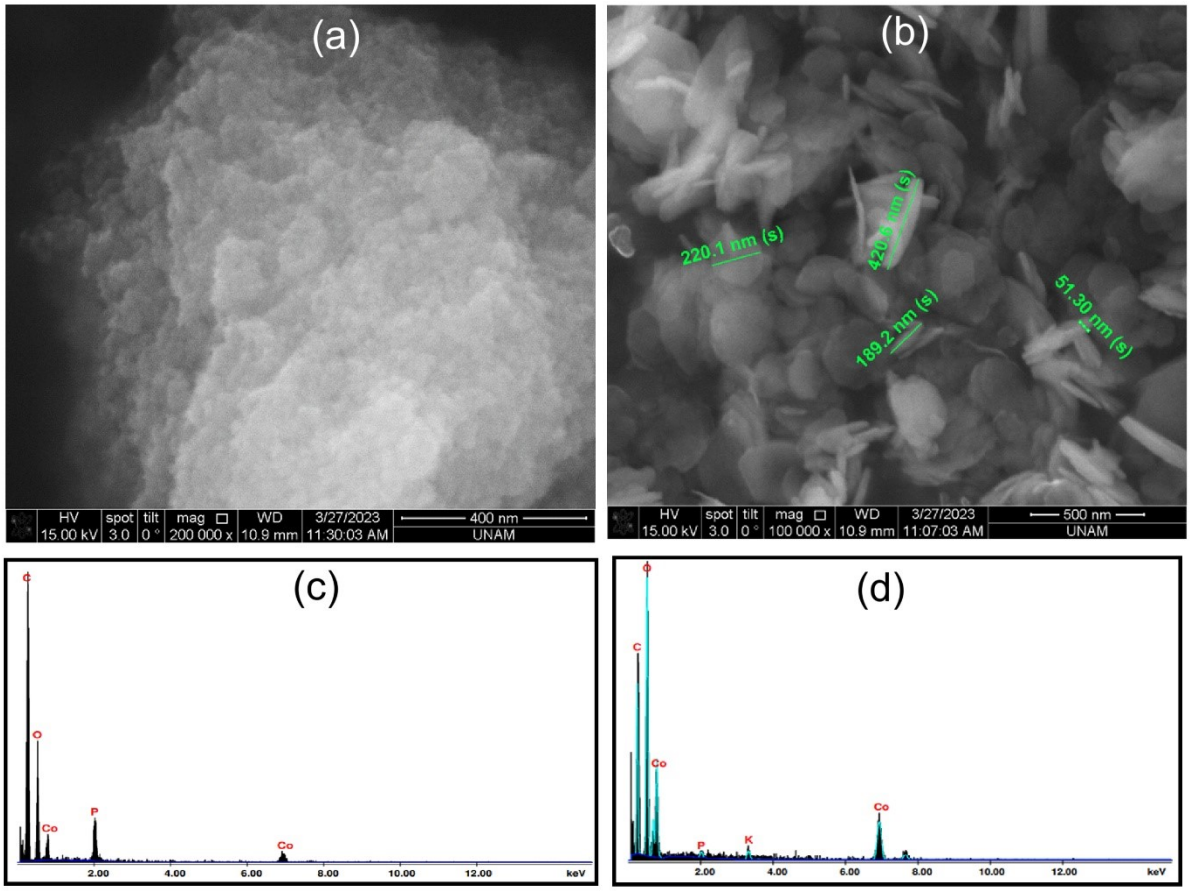

Figure S11. Before and after 1 M KOH treatment of $Co_2P_2O_7$ (a and b) SEM images and (c and) EDX spectra.

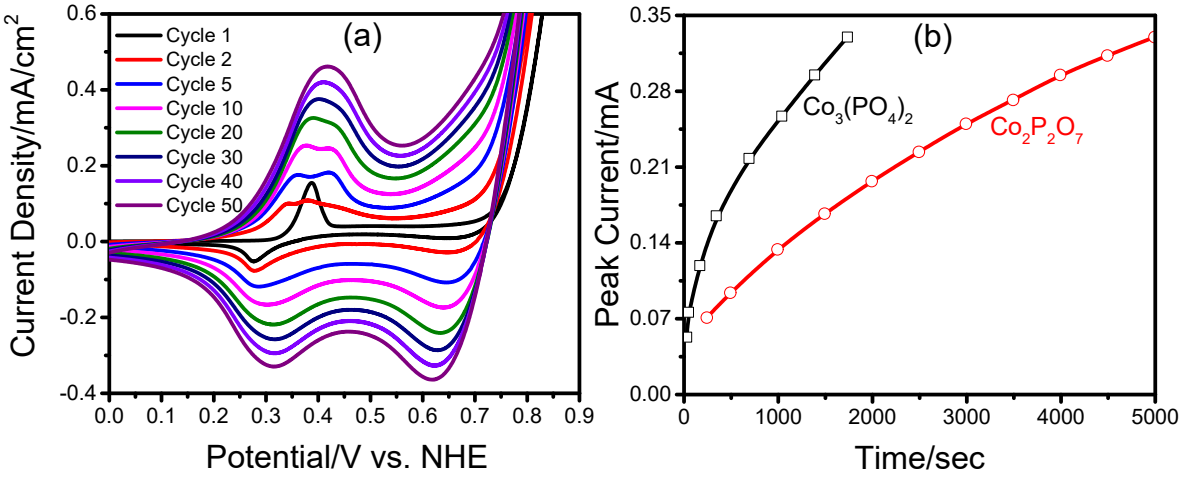

Figure S12. (a) Selected CVs from 50 CV cycles in 0.05 M KOH electrolyte solution and (b) plot of peak current at aroun 0.285 V versus CV cycle number of $Co_3(PO_4)_2$ electrode.

References

1) Pang, H. *et al.* Cobalt Pyrophosphate Nano/microstructures as Promising Electrode Materials of Supercapacitor. *J. Solid State Electrochem.* **2013**, *17*, 1383.
2) Khan, Z. *et al.* Redox-Additive-Enhanced High Capacitance Supercapacitors Based on $Co_2P_2O_7$ Nanosheets. *Adv. Mater. Interfaces* **2017**, *4*, .
3) Agarwal, A.; Majumder, S.; Sankapal, B. R. Carbon Nanotube-Functionalized Surface-Assisted Growth of Cobalt Phosphate Nanodots: A Highly Stable and Bendable All-Solid-State Symmetric Supercapacitor. *Ener. Fuels* **2022**, *36*, 5953.
4) Aydın, H.; Kurtan, Ü.; Üstün, B.; Koç, S. N. One-Pot Synthesis of Cobalt Pyrophosphate Nanoparticles Combined with Mesoporous Carbon for Asymmetric Supercapacitors. *Mater. Chem. Phys.* **2022**, *290*, .
5) Mangate, N. V.; Giripunje, S. M.; Kondawar, S. B. Electrospun 1D Cobalt Pyrophosphate Porous Nanofibers: Redox-Active Electrode Material for Asymmetric Supercapacitor. *J. Ener. Stor.* 2023, **67**, .
6) Ulu, I.; Ulgut, B.; Dag, Ö. Nanoarchitectonics of Mesoporous $M_2P_2O_7$ (M = Mn(II), Co(II), and Ni(II)) and $M_{2-x}Co_xP_2O_7$ and Transformation to Their Metal Hydroxides with Decent Charge Capacity in Alkali Media. *Inorg. Chem.* **2023**, *62*, 16994.
7) Marje, S. J.; Katkar, P. K.; Pujari, S. S.; Khalate, S. A.; Lokhande, A. C.; Patil, U. M. Regulated Micro-Leaf Like Nickel Pyrophosphate as a Cathode Electrode for Asymmetric supercapacitor, *Synth. Met.* **2020**, *259*, 116224.
8) Wei, C.; Cheng, C.; Wang, S.; Xu, Y.; Wang, J.; Pang, H. Sodium-Doped Mesoporous $Ni_2P_2O_7$ Hexagonal Tablets for HighPerformance Flexible All-Solid-State Hybrid Supercapacitors. *Chem. Asian J.* **2015**, *10*, 1731.
9) Wei, C.; Yang, S.; Liu, W.; Hou, X.; Sun, Y.; Zhao, J.; Xiong, W.; Cheng, C.; Zhang, D. Hierarchically Porous Bowknot-like Sodium Doped $Ni_2P_2O_7$-$Co_2P_2O_7$ with Improved Supercapacitor Performances. *Appl. Surf. Sci.* **2019**, *465*, 763.

10) Senthilkumar, B.; Khan, Z.; Park, S.; Kim, K.; Ko, H.; Kim, Y. Highly Porous Graphitic Carbon and $Ni_2P_2O_7$ for a High-Performance Aqueous Hybrid Supercapacitor. *J. Mater. Chem. A* **2015**, *3*, 21553.
11) Nivetha, S.; Prabahar, S.; Karunakaran, R. T.; Ganth, M. N.; Dhinesh, S. Synthesis and Characterization of $Ni_2P_2O_7$ Thin Film as a Superier Electrode Materials for high Performance Supercapacitors. *Ionics* **2023**, *29*, 1209.
12) Ulu, I.; Ulgut, B.; Dag, Ö. Fabrication of Mesoporous Nickel Pyrophosphate Electrodes and Their Transformation to Nickel Hydroxide with Decent Capacitance in Alkaline Media. *J. Mater. Chem. A* **2023**, ***11***, 22384.
13) Nair, M. S. S.; Sivakumar, T.; Venkateshwari, P. Regulated Micro-Balls Like Nickel Pyrophosphate/reduced Graphene Oxide ($Ni_2P_2O_7$@RGO) Composite Thin Films as a Cathode Electrode for Asymmetric Supercapacitor. *J. Mater. Sci: Mater. Electron.* **2025**, *36*, 1055.
14) BoopathiRaja, R.; Vadivel, S.; Parthibavarman, M.; Prabhu, S.; Ramesh, R. Effect of Polypyrrole Incorporated Sun Flower Like $Mn_2P_2O_7$ with Lab Waste Tissue Paper Derived Activated Carbon for Asymmetric Supercapacitor Aplications. *Surfaces Interfaces* 2021, **26**, 101409.
15) Pang, H. et al. Template-free Controlled Fabrication of $NH_4MnPO_4{\cdot}H_2O$ and $Mn_2P_2O_7$ Micro-Nanostructures and Study of Their Electrochemical Properties. *Int. J. Electrochem. Sci*. **2012**, *7*, 12340.
16) AZhao, Y.F.; Chen, S.Q.; Sun, B.; Su, D.W.; Huang, X.D.; Liu, H.; Yan, Y.M.; Sun, K.N.; Wang, G.X. Graphene-Co_3O_4 Nanocomposite as Electrocatalyst with High Performance for Oxygen Evolution Reaction. *Sci. Rep.* **2015**, *5*, 7629.
17) Du, S. C.; Ren, Z. Y.; Zhang, J.; Wu, J.; Xi, W.; Zhu, J. Q.; Fu, H. G. Co_3O_4 Nanocrystal Ink Printed on Carbon Fiber Paper as a Large-Area Electrode for Electrochemical Water Splitting. *Chem. Commun.* **2015**, *51*, 8066.
18) Nai, J. W.; Yin, H. J.; You, T. T.; Zheng, L. R.; Zhang, J.; Wang, P. X.; Jin, Z.; Tian, Y.; Liu, J. Z.; Tang, Ni, B.; Wang, X. Edge Overgrowth of Spiral Bimetallic Hydroxides Ultrathin-Nanosheets for Water Oxidation. *Chem. Sci.* **2015**, *6*, 3572.
19) Jiang, J.; Zhang, A.; Li, L.; Ai, L. Nickel–Cobalt Layered Double Hydroxide Nanosheets as High-Performance Electrocatalyst for Oxygen Evolution Reaction. *J. Power Sources* **2015**, *278*, 445.
20) Ni, Y.; Shi, D.; Mao, B.; Wang, S.; Wang, Y.; Ahmad, A.; Sun, J.; Song, F.; Cao, M.; Hu, C. Under-Coordinated CoFe Layered Double Hydroxide Nanocages Derived from Nanoconfined Hydrolysis of Bimetal Organic Compounds for Efficeint Electroctalytic Water Oxidation. *Small* **2023**, 2302556.
21) Jena, R. *et.al.* In Situ Tracking of Ni-MOF Reconstruction into Active $Ni(OH)_2$ OER Catalysts**.** *Angew. Chem. Int. Ed.* **2025,** *64*, e202510741**.**
22) Zhang, W. et al. A Thin NiFe Hydroxide Film Formed by Stepwise Electrodeposition Strategy with Significantly Improved Catalytic Water Oxidation Efficiency. *Adv. Energy Mater.* **2017**, *7*, 160254.
23) Lu, X.; Zhao, C. Electrodeposition of Hierarchically Structured Three-dimensional Nickel–iron Electrodes for Efficient Oxygen Evolution at High Current Densities. *Nature Commun.* **2015**, *6*, 6616.
24) Gao, M. *et al.* Efficient water oxidation using nanostructured α-nickel-hydroxide as an electrocatalyst. *J. Am. Chem. Soc.* **2014**, *136*, 7077.
25) Kang, B. K. *et al.* Mesoporous Ni-Fe oxide multi-composite hollow nanocages for efficient electrocatalytic water oxidation reactions. *J. Mater. Chemistry A* **2017**, *5*, 4320.

26) Katırcı, A. A.; Durukan, I. K.: Dag, Ö. Nanoarchitectonic Mesoporous $Ni_{1-x}Mn_xO$ Electrodes: Charge Capacity and Oxygen Evolution Reaction Electrocatalysis in Alkaline Media. *ACS Appl. Energy Mater.* **2025**, *8*, 3162.
27) Ceran, G.; Durukan, I. K.; Ulu, I.; Dag, Ö. Scalable Solvent-Mediated Nanoarchitectonics of High–Surface-Area Mesoporous $Ni_2P_2O_7$ for Enhanced Electrochemical Performance in Alkaline Media. *Inorg. Chem.* **2025**, doi.org/10.1021/acs.inorgchem.5c05373, in press.
28) Meng, Y.; Song, W.; Huang, H.; Ren, Z.; Chen, S. Y.; Suib, S. L. Structure–Property Relationship of Bifunctional MnO_2 Nanostructures: Highly Efficient, Ultra-Stable Electrochemical Water Oxidation and Oxygen Reduction Reaction Catalysts Identified in Alkaline Media. *J. Am. Chem. Soc.* **2014**, *136*, 11452.
29) Fekete, M.; Hocking, R. K.; Chang, S. L. Y.; Italianoe, C.; Patti, A. F.; Arena, F.; Spiccia, L. Highly Active Screen-Printed Electrocatalysts for Water Oxidation Based on β-Manganese Oxide. *Energy. Environ. Sci.* **2013**, *6*, 2222.
30) Tian, L.; Zhai, X.; Wang, X.; Pang, X.; Li, J.; Li, Z. Morphology and Phase Transformation of α-MnO_2/MnOOH Modulated by N-CDs for Efficient Electrocatalytic Oxygen Evolution Reaction in Alkaline Medium. *Electrochim. Acta* **2020**, *337*, 135823.
31) Kölbach, M.; Fiechter, S.; van de Krol, R.; Bogdanoff, P. Evaluation of Electrodeposited α-Mn_2O_3 as a Catalyst for the Oxygen Evolution Reaction. *Catal. Today* **2017**, *290*, 2.
32) Walter, C.; Kalra, S.; Beltrán-Suito, R.; Schwarze, M.; Menezes, P. W.; Driess, M. Manganese Sulfide Enables the Formation of a Highly Active β-MnOOH Electrocatalyst for Effective Alkaline Water Oxidation. *Mater. Today Chem.* **2022**, *24*, 100905.
33) Zhao, Y.; Chang, C.; Teng, F.; Zhao, Y.; Chen, G.; Shi, R.; Waterhouse, G. I. N.; Huang, W.; Zhang, T. Defect-Engineered Ultrathin δ-MnO_2 Nanosheet Arrays as Bifunctional Electrodes for Efficient Overall Water Splitting. *Adv. Energy Mater.* **2017**, *7*, 1700005.
34) Ahmed, A. T. A.; Ansari, A. S.; Cho, S.; Jana, A. Morphology and Surface Reconstruction-Driven Catalytic Enhancement in $CoMn_2O_4$ for Efficient OER Application. *Materials* **2026**, *19*, 542.
35) Fan, W. *et al.* Dual-defects Stimulating catalytic site activity to enhance oxygen evolution performance of cobalt oxide. *Fuel* **2026**, *404*, 136300.
36) Qi, S. *et al.* Switching the Oxygen Evolution Reaction Mechanism through the Creation of Disordered NiOOH Induced by Electrochemical Reconstruction. *Adv. Mater.* **2026**, *38*, e12188.
37) Tang, Z. *et al.* Iron incorporation and sulfur modification synergistically enhance oxygen evolution in nickel–cobalt hydroxide electrocatalysts. *J. Solid State Chem*. **2026**, *356*, 125807.
38) Yang, C. Y. *et al.* Binary ruthenium dioxide and nickel oxide ultrafine particles loaded on carbon nanotubes for high-stability oxygen evolution reaction at high current densities. *J. Colloid Interface Sci*.**2025**, *677*, 323.